Bull Earthquake Eng
DOI 10.1007/s10518-017-0152-4

ORIGINAL RESEARCH PAPER

Assessing seismic hazard of the East African Rift: a pilot study from GEM and AfricaArray

Valerio Poggi[1] · Raymond Durrheim[2] · Georges Mavonga Tuluka[3] · Graeme Weatherill[1] · Robin Gee[1,6] · Marco Pagani[1] · Andrew Nyblade[2,4] · Damien Delvaux[5]

Received: 19 December 2016 / Accepted: 5 May 2017

Abstract The East African Rift System is the major active tectonic feature of the Sub-Saharan Africa region. Although the seismicity level of this divergent plate boundary can be described as moderate, several damaging earthquakes have been reported in historical times, and the seismic risk is exacerbated by the high vulnerability of the local buildings and structures. Formulation and enforcement of national seismic codes is therefore an essential future risk mitigation strategy. Nonetheless, a reliable risk assessment cannot be done without the calibration of an updated seismic hazard model for the region. A major limitation affecting the assessment of seismic hazard in Sub-Saharan Africa is the lack of basic information needed to construct source and ground motion models. The historical earthquake record is sparse, with significant variation in completeness over time across different regions. The instrumental catalogue is complete down to sufficient magnitude only for a relatively short time span. In addition, mapping of seismogenically active faults is still an on-going task, and few faults in the region are sufficiently constrained as to allow them to be directly represented within the seismic hazard model. Recent studies have identified major seismogenic lineaments, but there is substantial lack of kinematic information for intermediate-to-small scale tectonic features, information that is essential for the proper calibration of earthquake recurrence models. In this study, we use new data and Global Earthquake Model (GEM) computational tools such as the Hazard Modeller's Toolkit and the *OpenQuake* engine to perform a pilot study of the seismic hazard associated with the East African Rift. The hazard model obtained has been created using the

✉ Valerio Poggi
valerio.poggi@globalquakemodel.org

[1] Global Earthquake Model Foundation (GEM), Pavia, Italy

[2] University of the Witwatersrand, Johannesburg, South Africa

[3] Goma Volcanic Observatory, Goma, Democratic Republic of the Congo

[4] Pennsylvania State University, State College, PA, USA

[5] Royal Museum for Central Africa, Tervuren, Belgium

[6] Istituto Nazionale di Oceanografia e di Geofisica Sperimentale (OGS), Trieste, Italy

Published online: 12 May 2017

most recent information available from scientific literature, global bulletins and local earthquake catalogues, including those from *AfricaArray* projects. In this report, in accordance with the GEM philosophy, we describe in detail all working assumptions, main processing steps, data analyses and interpretations used for the model setup.

Keywords Probabilistic seismic hazard analysis · GMPEs · Uncertainty analysis · Earthquake engineering · Logic-tree

1 Introduction

Earthquakes pose a significant risk in many regions of the Sub-Saharan Africa (SSA), more particularly along the tectonically active East African Rift System (EARS). Further away from this rift system, the remainder of SSA is largely considered a stable intra-plate region characterized by a relatively low rate of seismicity. Nonetheless, several large earthquakes have been reported in historical times. While most of earthquakes in Sub-Saharan Africa occur along the EARS (inter-plate seismicity), it must be noted that a damaging earthquake can occur anywhere, especially as cities grow and many buildings are constructed without taking potential ground shaking into account. Even moderate-sized events can prove disastrous should it occur near a city with many vulnerable buildings, as happened when a M_W 5.7 earthquake struck Agadir, Morocco in 1960, causing some 15,000 deaths.

Damaging earthquakes with $M > 6$ occur almost annually in the East African Rift, and five $M > 7$ earthquakes have occurred in eastern Africa since 1900. The largest known event in the region is the 13 December 1910 M_S 7.4 Rukwa (Tanzania) event that badly cracked all European-style houses in towns on the eastern shore of Lake Tanganyika (Midzi and Manzunzu 2014; Ambraseys 1991a; Ambraseys and Adams 1991). A M_S 6.9 earthquake that occurred on 6 January 1928 in the Subakia Valley (part of the Kenya Rift, some 200 km northwest of Nairobi) produced a 38 km long surface rupture with a maximum throw of 2.4 m and destroyed, or damaged beyond repair, all European-style houses within 15 km of the rupture, fortunately without causing casualties (Ambraseys 1991b).

During the last decade several other events caused loss of life (Durrheim 2016). On 5 December 2005 a M_W 6.8 event caused several deaths and damaged school buildings and hundreds of dwellings in the Democratic Republic of Congo (DRC) and western Tanzania. The 22 February 2006 Mozambican M_W 7 earthquake was one of the largest ever recorded in Southern Africa, producing a surface rupture with a displacement of more than 1 m (Fenton and Bommer 2006). Shaking was felt as far away as Zimbabwe and South Africa. Four people were killed, 27 injured, and at least 160 buildings damaged. On 3 February 2008 a M_W 5.9 earthquake struck the Lake Kivu region of the DRC and neighbouring Rwanda. The event was located near Bukavu (d'Oreye et al. 2008), now with a population of 700,000, and can be regarded as a "near miss". A second earthquake followed the main shock 3 1/2 h later. Numerous buildings collapsed or suffered significant structural damage, trapping many people under rubble. At least 40 people died and more than 400 were injured. Even more recently, a M_W 5.9 earthquake that occurred on 10 September 2016 near the west shore of Lake Victoria in northern Tanzania (some 200 km to the east of the West Branch of the Rift System) caused more than a dozen fatalities and 200 injuries (USGS 2016), in a region which was previously devoid of instrumental seismicity.

While these events caused relatively small losses, the population of the region has increased enormously over the last century and increasingly urbanized; trends that are expected to continue well into the mid-21st century. Building methods have changed from wattle and daub or timber with grass roofs, which have a large inherent resistance to earthquake shaking, to European-style unreinforced masonry constructions, which are far more vulnerable to shaking (Brzev et al. 2013). The occurrence of similar events close to a town would likely cause serious human and economic losses today.

The mitigation of earthquake risk in Africa requires coordinated action on several fronts. Firstly, seismic hazard assessments should be improved by maintaining and expanding seismic monitoring networks, supplementing historical and paleoseismic catalogues, and mapping active faults at the near-surface. Secondly, building codes should be formulated and enforced, and vulnerable existing buildings and infrastructure reinforced to prevent serious damage or collapse when subjected to strong shaking. Lastly, disaster management agencies, emergency first responders, and the general public should be trained to act effectively and sensibly during an earthquake, and equipped to deal with the aftermath. National efforts to assess and address the risks posed by earthquakes are reviewed by Worku (2014) and Lubkowski et al. (2014).

In this paper, we illustrate part of the activities completed within a USAID-funded pilot project, where we seek to gain knowledge and build capacity to mitigate and reduce seismic risk in regions affected by earthquakes associated with the East African Rift System. Within this framework, a regional probabilistic seismic hazard model based on distributed seismicity has been developed and is discussed.

2 Tectonics and morphology of the East African Rift System

The African continent is a palimpsest recording a lengthy tectonic history, and the East African Rift System (EARS) is superimposed on structures formed during earlier tectonic episodes (McConnell 1980). On a broad scale, much of it can be explained by plate tectonics and the Wilson cycle, for example the amalgamation and dispersal of Gondwana. However, there are other phenomena, such as the rise of the African Superswell (Nyblade and Robinson 1994), that are not yet fully understood.

The EARS is an outstanding example of an active continental rift system. This divergent plate boundary runs roughly NS through eastern Africa, separating the Nubian and Somalian plates. It intersects the Afar depression in northern Ethiopia, where a triple-junction connects it north-west to the Red Sea rift and north-east to the Gulf of Aden rift, which extends then as far as the Indian Ocean Ridge. Towards the south, the EARS splits into two branches—the eastern and western rifts—that bracket the Tanzanian craton. The eastern rift extends along the coast of Mozambique, veers into the Indian Ocean, and eventually joins the Southwest Indian Ocean Ridge (SWIR). The western rift continues through Lake Malawi into central Mozambique, with several splays that extend into continental Africa.

The EARS was likely initiated in the region of the present-day Turkana Rift (Furman et al. 2006) during the mid-Tertiary (Macgregor 2015). After a first volcanic phase, tectonic activity progressively migrated towards the north triggering uplift, extrusion of flood basalts (Pik et al. 2003) and consequent development of the Ethiopian plateau—which is world's youngest continental flood basalt province—and of the Main Ethiopian Rift (Saria et al. 2014). The Western branch of the EARS formed subsequently (Roberts et al. 2012;

Macgregor 2015) around 25 Myr, simultaneously with the Eastern branch, within a spreading process that is still on going and is responsible for the largest seismicity experienced in the Africa continent.

From the seismological point of view, the region is characterised by large intrinsic attenuation, due to the presence of a low-velocity anomaly in the lower mantle, named the African superplume (e.g., Ritsema et al. 1998; Gurnis et al. 2000; Simmons et al. 2007; Hansen et al. 2012), which is also thought to be responsible of the high topographic elevation of the region (e.g., Nyblade and Robinson 1994; Lithgow-Berteloni and Silver 1998; Saria et al. 2014) and the associated volcanism.

3 Seismic hazard analysis: methodology

Seismic Hazard is evaluated for the regions surrounding the EARS by developing a probabilistic model based on distributed seismicity sources. The choice of this source type was mostly driven by current data, including local earthquake catalogues, faults, and focal mechanisms. Consideration was also given to a regional strain rate model developed for the area by Stamps et al. (2015) in the frame of the *GEM Strain Rate Project*.

For a given site, the distributed seismicity approach determines the probabilities of exceeding, at least once in a given time span, a set of ground motion levels of engineering interest generated by a number of seismically and tectonically homogenous earthquake source zones. In its simplest representation, each source is considered independent from others and the earthquake rupture process within zones is assumed to follow a *Poisson* process. More comprehensive descriptions of Probabilistic Seismic Hazard Analysis (PSHA) can be found for example in Field et al. (2003), McGuire (2004) and USNRC (2012). Calculation of seismic hazard is made through the use of the *OpenQuake*-engine (Pagani et al. 2014), an open source seismic hazard and risk calculation software developed, maintained and distributed by the Global Earthquake Model.

4 The SSA-GEM earthquake catalogue

The starting point for any PSHA is the definition of the seismicity characteristics, in terms of both the long-term recurrence as well as the seismotectonic properties (e.g. style of faulting, depth distribution etc.), for the study area. This can be done in multiple ways, but the basic—and probably the most common—approach is in the use of an earthquake catalogue. For the purposes of constraining earthquake recurrence, it is critical to identify which portions of the catalogue can be considered to be a complete record of all earthquake events indirectly reported (the historical and macroseismic component) or directly recorded (the instrumental component) on a specific area and over a certain time span.

If several catalogues are available for a given study area, information (location solutions, reported time, intensity scale) can be quite heterogeneous and some objective criteria for selection, merging and homogenisation are needed. This is usually the case when different agencies are reporting the same events but with different magnitude types. The same issue affects source solutions, for instance when different earthquake phases, processing algorithms or base model assumptions (e.g. earth velocity structure) are used.

GEM has recently developed a set of open-source tools that helps scientists go through the catalogue harmonisation process. In this study we make use of these tools (aka GEM

Catalogue Toolkit, Weatherill et al. 2016) to produce an up-to-date earthquake catalogue for Sub-Saharan Africa with homogenous magnitude representation (M_W). Such catalogue (hereinafter SSA-GEM) is obtained by augmenting available global catalogues (e.g. ISC-Reviewed, ISC-GEM, GCMT) with information from local agencies and regional projects, particularly from *AfricaArray* temporary deployments (e.g. Mulibo and Nyblade 2013, 2016). In the following we describe in detail the necessary steps, main assumptions and choices we faced to set up the SSA-GEM catalogue, in accordance with the GEM philosophy of complete disclosure of processing procedures.

4.1 Source data

4.1.1 ISC reviewed bulletin

The manually reviewed bulletin from the International Seismological Centre (ISC 2013) was used as one of the primary sources of information for the earthquake catalogue. The ISC bulletin covers a period ranging from the beginning of the 20th century to present day. In our selected geographic area (−40° to 20° North, 10° to 60° East) it spans the period 1904–2013, and includes a total of 26,322 events from 89 international and national (local) agencies. Magnitude scale representation is, however, not homogenous and varies between agencies and time periods.

4.1.2 ISC-GEM catalogue

The ISC-GEM global instrumental earthquake catalogue (Storchak et al. 2013, 2015) is a refined version of the ISC bulletin, which improves the accuracy of magnitude and location solutions for large global events ($M_W > 5.5$) in the period 1900–2012. Events reported in the ISC-GEM catalogue are considered as reference events, which have priority over other estimates from global bulletins. Earthquake size is homogeneously represented by using moment magnitude (M_W) from globally calibrated magnitude conversion relations. The ISC-GEM catalogue is presently in its version 3, which is the one used in this study. 285 events (out of 24,375) fall within the selected study region.

4.1.3 Harvard/GCMT bulletin

The Global Centroid Moment Tensor catalogue (GCMT, Ekström et al. 2012) is a collection of moment tensor solutions for earthquakes with $M_W > 5$. The catalogue covers the period 1976 to present, with a total of more than 40,000 global events, 614 of which are of interest for this study. Note that within the ISC bulletin, the Global Centroid Moment Tensor catalogue is indicated with two separated agency labels, HRVD and GCMT, indicating the migration of the project from Harvard (Harvard CMT Project) to the Lamont–Doherty Earth Observatory (LDEO) of the Columbia University in 2006. Moment tensor solutions from the GCMT are considered as reference for the calibration of magnitude conversion relations used in this study.

4.1.4 GEM historical earthquake archive

The GEM Historical Earthquake Catalogue (GEH) is a global collection of reviewed historical records consisting of 825 events ($M > 7$) covering the period 1000–1903 (pre

instrumental period). Only eight earthquakes from the GEH catalogue fall within the study region. The small number is likely due to the lack of historical records in sub-Saharan Africa, and poses the problem of completeness of the regional earthquake record for large magnitudes, which may consequently bias the calibration of annual occurrence rates for these events.

4.1.5 AfricaArray and regional earthquake catalogues

We extended the earthquake record by integration of three local catalogues. These catalogues are the result of regional earthquake monitoring performed with temporary and permanent seismic network installations.

1. The Tanzanian Broadband Seismic Experiment (TZB), with 2218 events covering the period 1994–1995 and M_S magnitude between 1.43 and 4.42 (Langston et al. 1998);
2. The Ethiopian Plateau Catalogue (ETP), with 253 events covering the period 2001–2002 and with M_S magnitude between 1.75 and 4.05 (Brazier et al. 2008);
3. The *AfricaArray* Eastern Africa Seismic experiment (AAE), with 1023 events in the period 2009–2011 and M_S magnitude range 1.28–4.04 (Mulibo and Nyblade 2016).

Although these catalogues extend the record to very low magnitudes, their primary application within the present hazard study was for the local definition of seismicity distribution patterns in order to elucidate potentially seismogenic structures within the rift system and the surrounding regions. Subsequently, these are used to improve the design of a new area source model for Sub-Saharan Africa.

4.2 Location solution

In many applications, preference for earthquake location solution should be given to local agencies, while solutions from global agencies and teleseismic events should be alternatively used in those cases where local agencies are not available on the territory (e.g. not yet established) or where large solution uncertainty exists, e.g. due to insufficient station coverage. For the case of Sub-Saharan Africa, although solutions from several local agencies are made available through the ISC bulletin, there is general lack of information regarding network operation (particularly before 1980) and metadata—including the quality of the solutions—which makes the use of their locations often questionable. Nonetheless, events recorded teleseismically are unlikely to be affected by changes in station location or operation over time, with a consequent decreased bias in the solution error for different periods of the catalogue.

For these reasons, solutions from global agencies have been preferred, while the use of solutions produced by local agencies was restricted to those cases where no other information was available. By mapping the activity period of the different seismological agencies over time and through the use of available network information from literature, technical reports and local experts, we identified five main time intervals and adopted a different agency prioritisation scheme for the selection of the best available location within each (see summary Table 1).

4.3 Magnitude homogenisation

An unbiased seismicity analysis requires that the seismic record is represented homogeneously in terms of the magnitude scale, to avoid inconsistencies due to the different

Table 1 Prioritisation of agencies for preferred location solution

Period	Agency priority list
1000–1900	GEH
1901–1959	ISC-GEM, ISC, ISS, GUTE, GEH
1960–1964	ISC-GEM, EHB, ISC, ISS, GEH
1965–1980	EHB, ISC, NEIC, IDC, GCMT, HRVD, GCMT-NDK, BUL, PRE, LSZ, TAN, CNG, GEH
1981–2015	EHB, ISC, NEIC, IDC, GCMT, HRVD, GCMT-NDK, AAE, ETP, TZB, PRE, LSZ, NAI, TAN, CNG, EAF, GEH

Selection is done differently for separated time periods, accounting for network operation and reliability of the estimate. We refer to ISC website (http://www.isc.ac.uk/iscbulletin/agencies, last access August 2016) for acronyms not otherwise described in the article

processing schemes used for the calculation of different magnitude scales and the manifestation of saturation effects. Among the several scales that can possibly be used as reference, the most natural choice is moment magnitude (M_W), due to its direct connection to earthquake size and energy, and the absence of saturation at high magnitudes. However, events with a native estimate of M_W (i.e. directly obtained from data) are limited, and very often a conversion from other scales is necessary.

Calibration of regional conversion rules from local datasets is generally advisable; however, it can be limited by availability of events with multiple magnitude scale representations. Alternatively, a two- (or three-) step conversion with an intermediate dummy magnitude measure of larger availability can be used, with the drawback of the progressive accumulation of uncertainty at each conversion step. If no calibration data are available at all, globally calibrated conversion rules can still be applied.

For the definition of ad-hoc magnitude conversion rules, we used in this study the functionalities offered by the GEM catalogue toolkit (Weatherill et al. 2016), which allows for the exploration and statistical analysis of local, regional and global datasets to build statistical regression models for the magnitude conversion. In the SSA region, unfortunately, we experienced a substantial lack of calibration data to implement local M_W conversion rules and in several cases we had to rely on globally calibrated relations (see Table 2).

4.4 Duplicate findings and catalogue homogenisation

When merging different earthquake catalogues, one issue is the identification of duplicate events. To face this problem, events falling within a window of prescribed spatial and temporal width are assumed to represent the same earthquake. Best results have been obtained with a window of 0.5° and 120 s. These values appear sufficient to capture relative uncertainty in earthquake solution between agencies, which is particularly relevant for teleseismic events. The use of larger values had led to erroneous results, by misinterpreting earthquakes in aftershock sequences as duplicates. After catalogue merging, previously defined priority rules for magnitude and location agency selection are applied and the final catalogue is produced (Figs. 1, 2a).

Table 2 List of agencies and corresponding M_W conversion rules

Agency	M_W conversion rule	Range	References
ISC	$0.616M_S + 2.369$	$M_S < 6$	Weatherill et al. (2016)
	$0.994M_S + 0.1$	$M_S > 6$	
	$1.084m_b - 0.142$	$m_b < 6.5$	
NEIC	$0.723M_S + 1.798$	$M_S < 6.5$	
	$1.005M_S - 0.026$	$M_S > 6.5$	
	$1.159m_b - 0.659$	$m_b < 6.5$	
PRE	M_L	$M_L < 6$	Assumed 1:1 scaling and arbitrary uncertainty (0.3)
BUL	M_{blg}	$M_{blg} < 6$	
TZB, ETP, AAE	$1.02 + 0.47M_L + 0.05M_L^2$	$M_L < 5$	Edwards et al. (2010)
PAS	$0.616(M_S - 0.2) + 2.369$	$M_S > 6$	ISC-M_S corrected [as suggested in Engdahl and Villasenor (2002)]
	$0.994(M_S - 0.2) + 0.1$	$M_S < 6$	

Agencies are sorted according to decreasing priority for the catalogue harmonisation

4.5 Catalogue declustering

A widespread assumption in standard PSHA is that earthquake occurrence rates are independent of the observation time and that their probability distribution is that of a Poisson process. However, earthquake catalogues are naturally affected by the presence of groups of correlated events (clusters), such as fore- and aftershock sequences and seismic swarms, which are highly dependent in space and time.

In order to estimate Poissonian seismicity rates, those dependent events have to be removed by filtering the catalogue prior to the calibration of any occurrence relationship. Such procedure is called catalogue declustering and several algorithms have been proposed to address this issue (see Van Stiphout et al. 2012 for a review). Among others, one of the most popular is from Gardner and Knopoff (1974), due to its conceptual and computational simplicity. The algorithm isolates and removes dependent events from a sorted catalogue by virtue of a fixed time-distance window centred on each (assumed) earthquake main shock and proportional to its magnitude. Although several window variants exist (see Uhrhammer 1986; van Stiphout et al. 2012), we used the original magnitude-scaling relation of Gardner and Knopoff (1974). The declustered SSA-GEM catalogue consists of 7259 events out of the original 29,803 in the magnitude range $3 \leq M_W \leq 7.53$ (Fig. 2b).

5 Seismic source zonation

The proposed seismic source model for Sub-Saharan Africa is based on distributed seismicity sources, consisting of areal zones representing uniform temporal and spatial earthquake occurrence. This approach is commonly used when observed seismicity cannot be reliably linked to any known (or inferred) geologic structure, which is often the case in low-to-moderate seismicity regions. The main advantage of using area source zones (ASZ) lies in their flexibility with regard to the definition of the properties of seismogenesis within a region, and the possibility of varying their geometries to guarantee a sufficiently large set of earthquakes to be used for the characterisation of seismicity occurrence.

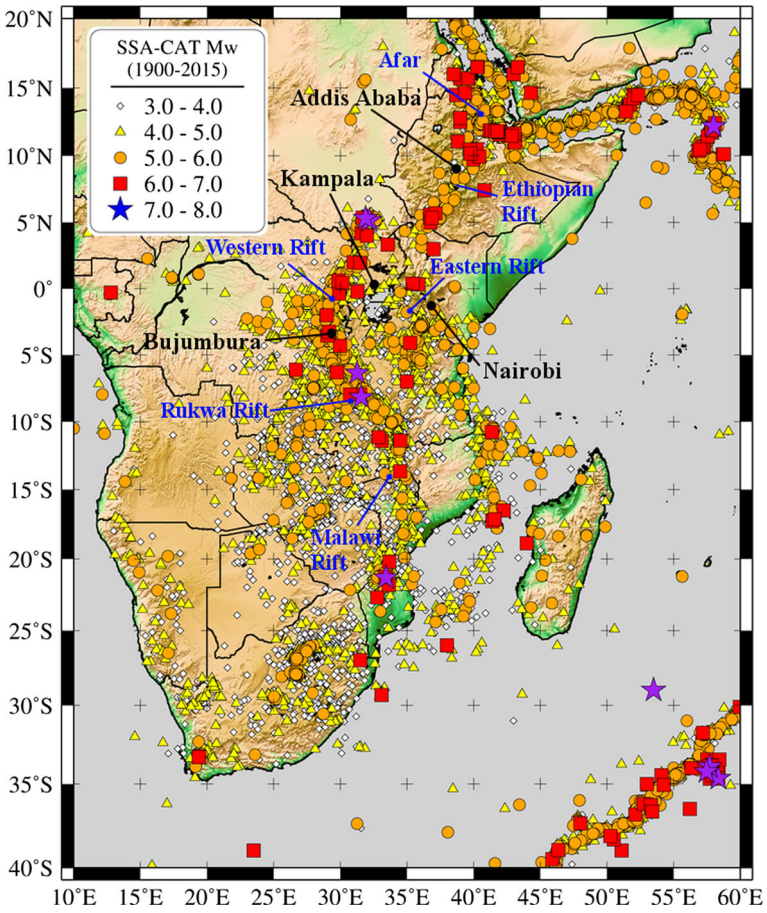

Fig. 1 Distribution of Earthquake events ($M_W \geq 3$) from the homogenised SSA-GEM earthquake catalogue. Names of the major rift systems associated with seismicity are indicated on the map with *blue labels*, while the four African capitals analysed at the end of this study are marked in *black*

However, the selection criteria may be highly subjective and in few cases experts may fail to reach consensus.

For the development of the area source model we followed a mixed approach, which accounts for both observed seismicity and the geological/tectonic characteristics of the study region. Such an approach closely follows from the methodology advocated by Vilanova et al. (2014), which consists in the definition of a set of objective criteria for the delineation of ASZ boundaries. Seismicity constraints have been obtained from the analysis (completeness, occurrence rates) of the SSA-GEM earthquake catalogue, which will be discussed in more detail in the next section. Tectonic information was derived mostly from scientific literature and by integration of available datasets.

The current area source model consists of a total of 19 zones distributed over 6 main tectonic groups (Table 3; Fig. 3), which we assume to have comparable rheological and mechanical behaviour with respect to the underlying crustal geology. The definition of these groups is essential for the regional calibration of *b*-values. Within five zones (7, 10,

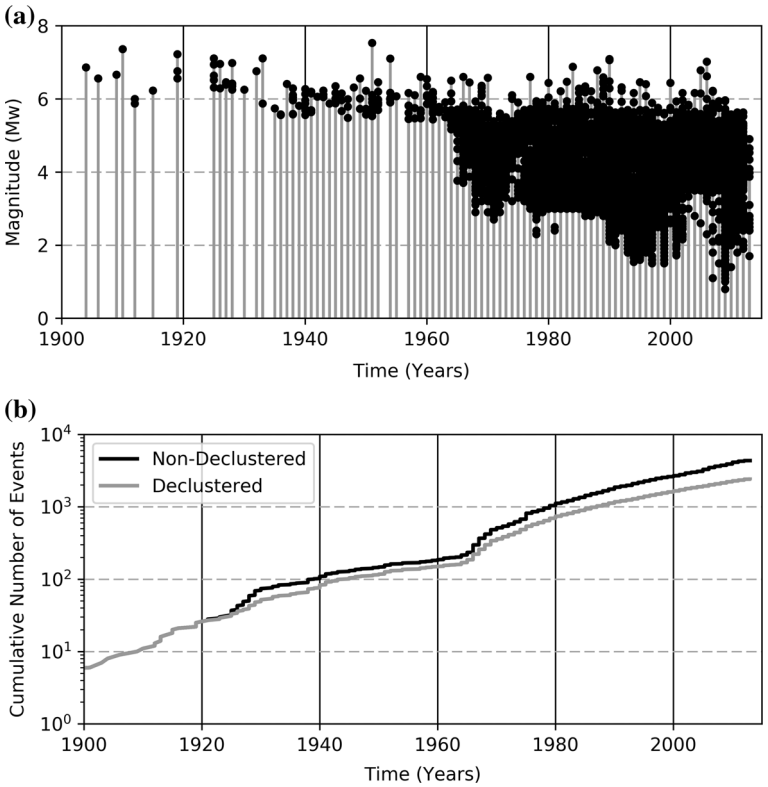

Fig. 2 **a** Distribution of seismicity over time for the events in the homogenised SSA-GEM earthquake catalogue. **b** Comparison between cumulative distribution of earthquakes before (non-declustered catalogue) and after fore-/aftershock cluster removal (declustered catalogue) for events larger than M_W 4.5 (lowest magnitude threshold considered for seismicity analysis). Historical events (before 1900) are not presented

11, 12, 13), we further define sub-regions with higher observed seismicity. We assume these layers (marked with the suffix .1) to inherit all the basic seismotectonic features of the containing (background) zone, but with occurrence rates adjusted to match non-uniform spatial distribution of local seismicity. In comparison to a smoothed seismicity approach, such method has the clear advantage of being better applicable in regions of low and sparse seismicity. Moreover it is possible to account for specific tectonic features when delineating the shape of the sub-zone. In the following section we describe in detail the main seismotectonic characteristics of each group.

5.1 Groups 1 and 2: Horn of Africa

The Afar triple junction is a key tectonic feature in the Horn of Africa, connecting the Arabian, Nubian and Somalian plates. It represents the point of accommodation of three connected extensional regimes, which are the Red Sea and Gulf of Aden spreading ridges to the north and the Ethiopian rift system to the south.

The area around the triple junction is characterised by significant seismic activity and several large earthquakes have been observed in historical and modern times. Surface geology and focal mechanisms of earthquakes show that the region is dominated by normal

Table 3 Source zones of the current SSA model assembled into tectonic groups

Group	Source zone	Name
1	2	South Red Sea
	3	Gulf of Aden
2	1	Afar depression–Eritrea
	4	Main Ethiopian Rift
	22	North Kenya–Lake Turkana
3	7, 7.1	Lake Victoria
	14	South Kenya
	20	Rovuma Basin
4	5	South Sudan
	6	Western Rift–Lake Albert to Kivu
	8	Western Rift–Tanganyika
	9	Rukwa–Malawi (Nyasa) Rift
	18	South Mozambique
5	10, 10.1	Walikale–Masisi
	11, 11.1	Upemba Graben
	12, 12.1	Mweru–South Katanga
	13, 13.1	Kariba–Okavango
6	15	Eastern Rift
	16	Davie Ridge
	17	Mozambique channel

faulting (e.g., Shudofsky 1985; Kebede and Kulhanek 1991; Ayele et al. 2006), with a minor although not negligible strike slip component. The triple junction extends to the Main Ethiopian Rift, a single extensional feature that separates the Nubian and Somalian plates (Wolfenden et al. 2004; Keir et al. 2009). Few earthquake focal mechanisms are available for the Main Ethiopian Rift, although most indicate normal faulting with an ESE–WNW orientation (Casey et al. 2006; Delvaux and Barth 2010). To the south is Lake Turkana, which is located in northern Kenya. The area surrounding this region exhibits the lowest seismicity within group 1 and 2, with a remarkable exception of the 1928 Subukia Earthquake (Ml 7.1, Mulwa et al. 2014).

We formally separate the marine Red Sea and Gulf of Aden source zones (which comprise group 1) from the inland source zones along the triple junction's southern branch that has not yet produced oceanic crust (Afar depression, Main Ethiopian Rift and the Lake Turkana depression of north Kenya, which comprise group 2). The rationale behind this choice lies in the likely different seismic attenuation behaviour of the two neighbouring regions. However, this hypothesis has to be confirmed by the analysis of local seismic recordings.

5.2 Group 3: African microplates

Between the Eastern and Western branches of the EARS is the Tanzanian craton, a large, stable portion of African lithosphere generally characterised by low seismicity. The craton is mostly comprised of Archean granitic-greenstones and high-grade metamorphic rocks (e.g., Chesley et al. 1999). Although the feature is considered tectonically stable and mostly inactive, some intraplate seismicity is recorded in the environs of Lake Victoria,

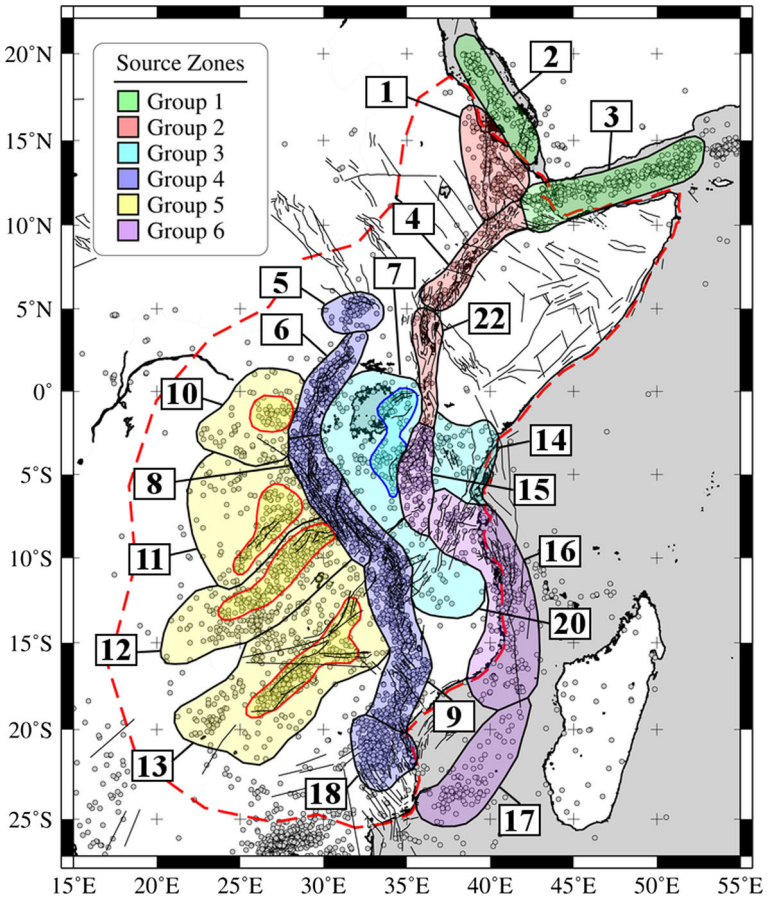

Fig. 3 Source zonation model used in this study (see Table 3 for details). Area sources belonging to same tectonic group are represented with unique colour. The outermost *red dashed line* marks the PSHA calculation area. Sub-regions of higher observed seismicity are marked with *thin coloured lines* for zones 7, 10, 11, 12 and 13. Plotted in the background are the SSA-GEM homogenised catalogue (non-declustered, Mw > 3) and the faults from the database of Macgregor (2015) used in this study

such as the Mw 5.9 event that occurred on 10 September 2016 (USGS 2016). Geophysical investigations have shown evidence of a rather thick lithosphere (150–200 km) below the craton (e.g. Petit and Ebinger 2000; Adams et al. 2012). Consequently, seismic attenuation is likely to be lower than in surrounding zones of active rifting (Saria et al. 2014).

Delineation of the source zones is predominantly based on the boundaries of microplates. Hartnady (2002) interpreted this region to be comprised of two distinct blocks, which are formally separated into the Victoria and Rovuma microplates based on their kinematic behaviour (Saria et al. 2014). The Victoria microplate consists mostly of the Tanzanian craton, and the Rovuma microplate boarders to the south and extends to northern Mozambique. A sub-region of higher seismicity has been defined within the group, situated west of the Gregory Rift in southern Kenya and Tanzania. Although this region has higher seismic productivity compared to other parts of the microplate, we assume it has a similar tectonic setting, making it suitable for the calculation of a common

b-value. Source group 3 also extends beyond the microplates to the eastern coast of Kenya and Tanzania, under the assumption that this region exhibits similarities to the rest of the source group, and is only separated geographically by the Eastern rift system.

5.3 Group 4: Western Rift System

The Western Branch of the EARS exhibits the highest rates of seismicity within the study area and limited volcanic activity. From north to south this source group includes the Albertine Rift (containing the Albertine Graben, Semliki Basin and Rwenzori Mountains), the Lake Kivu Basin including the Virunga volcanic area, and the Tanganyika-Rukwa-Malawi (TRM) rift segment (including Lake Tanganyika, the Mbeya triple junction and the Rungwe volcanic province). The Malawi Rift extends along the seismically active Urema graben towards south Mozambique, where the M_W 7.0 Machaze earthquake of 23 February 2006 occurred (Fenton and Bommer 2006; Yang and Chen 2010).

Seismicity in the Western Branch (i.e. centroid depths) extends through the entire crust and many of the larger earthquakes ($M > 6.5$) have nucleated within the lower crust (Nyblade and Langston 1995; Brazier et al. 2005; Craig et al. 2011), with hypocentres as deep as 30–40 km (Yang and Chen 2010). Unfortunately, the accuracy of the focal depth estimates is generally poor owing to the sparse station spacing (Mavonga and Durrheim 2009). The earthquake record is also largely incomplete before 1960 because of the substantial lack of seismic stations in the region.

Source group 4 contains five area sources, which cover several segments of the Western Branch, and delineation of the zones is predominantly based on fault orientations and stress patterns from inversion of focal mechanism data (Delvaux et al. 2012, 2016). The Albertine Rift is dominated by NE–SW normal faulting. The Lake Kivu area also displays normal faulting, but with a general NNE–SSW trend. Lake Tanganyika occupies the central part of the Western Branch, where the focal mechanisms in northern part of the lake indicate an ESE–WNW normal faulting regime with a slight strike slip component. The southern part of Lake Tanganyika belongs to the TRM zone, interpreted by Chorowicz (2005) as a the formation of an intercontinental transform extending south to Lake Malawi marked by a series of right lateral en-echelon faults. Delvaux et al. (2012) showed instead that the TRM segment currently opens in a NE–SW direction, orthogonal to the rift trend, and we have considered both interpretations in our source model by specifying a probability distribution for the rupture geometry that accounts for both rake and strike orientations. Within the TRM zone is the Kanda active fault system, located near the Rukwa Rift, which may have been responsible for the 1910 M_S 7.4 earthquake, the largest recorded in the East Africa Rift (Vittori et al. 1997; Delvaux et al. 2012).

5.4 Group 5: Central Africa

The Central Africa group encompasses the region west of the Western Rift, extending to parts of the Democratic Republic of Congo, Zambia, Zimbabwe, and Botswana. The northern area includes the very eastern Congo Basin (Masisi zone), where seismicity decreases moving away from the Western Rift (Delvaux et al. 2016). The southern zones are characterised by a series of NE–SW trending rifts (Upemba, Mweru, Kariba Rifts), striking roughly perpendicular to the Western Rift.

Four area sources are used to characterise this group, each with a sub-region of higher seismicity. The northernmost area, the Masisi zone, is located northwest of Lake Kivu. A study of earthquake focal mechanisms by Tanaka et al. (1980) showed that the direction of

the fault traces in that area is SE–NW, and the average focal mechanism is normal faulting with the tension axis perpendicular to the strike of the fault traces. The last strong earthquake occurred in the Masisi area on 29 April 1995 (M_b 5.1, Mavonga 2007; M_W 5.4, Barth et al. 2007). To the south, the most prominent seismotectonic features are the Upemba and Mweru Rifts (Kipata et al. 2013). The Upemba Rift is characterized by a NE–SW striking fault extending along its eastern side (Studt et al. 1908). It may extend northward to the Kabalo area, which experienced an earthquake with magnitude M_W 6.5 on 11 September 1992. Detailed investigation has revealed that the main geological features in the Kabalo area trend in the NNE–SSW direction, similar to those found in the Upemba Rift (Zana et al. 2004).

5.5 Group 6: Eastern Rift System

The Eastern Branch of the EARS extends from the rift systems of north Kenya to the offshore coast of Tanzania and Mozambique, along the Davie fracture zone. The northern segments can easily be tracked starting from the Turkana basin and moving southward along the system of rifts marking the eastern boundary of the Victoria microplate. Seismicity in the Eastern branch is less pronounced compared to its Western counterpart, and mostly concentrated in the southern segments (Manyara region). The segments of the Eastern branch are conversely characterised by a large volcanism (e.g., Dawson 1992; Yang and Chen 2010; Craig et al. 2011) that commenced about 25 Myr with the rifting of the Turkana region (Furman et al. 2006; McDougall and Brown 2009).

The source zones are mainly delineated based on seismic activity. South of the large seismicity gap that is observed along the Kenya and Gregory rifts, a zone of seismicity commences in central Tanzania (Macheyeki et al. 2008), representing the northernmost source zone in this group. The southern continuation of the Eastern Branch is however highly uncertain and the definition of the source zones is mostly controlled by the offshore seismic activity of Mozambique (Hartnady 1990; Hartnady et al. 1992), which is quite diffuse along the Davie Ridge (Grimison and Chen 1988; Franke et al. 2015) and its southern continuation.

6 Building the seismic source model

In this section we illustrate the process adopted for the construction of the earthquake source model. Each source in *OpenQuake* requires the characterisation of a three-dimensional finite rupture, whose properties are consistent with the seismotectonics of the region. A comprehensive description of an area source representation in *OpenQuake* can be found in Pagani et al. (2014).

6.1 Source depth distribution

A model for source depth distribution was derived based on the available information from the SSA-GEM catalogue. Unfortunately, not all reported events included an estimation of hypocentral depth solution. In few cases, although available, such estimate was considered unreliable because of the large uncertainty (generally at depths larger than 40 km) or because the depth was explicitly assigned a priori (e.g. fixed solution depths of 5, 10, 15

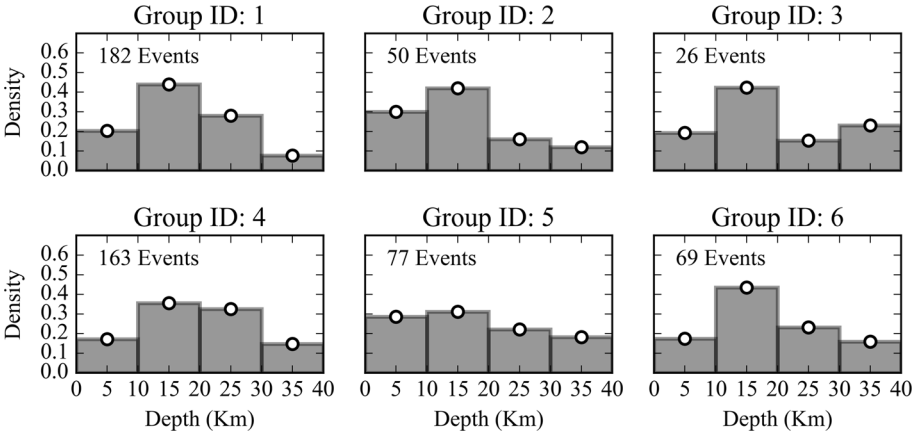

Fig. 4 Distribution of the hypocentral depth solutions of earthquake events falling into the main six source groups defined in Table 3. The largest contribution comes persistently from the depth range between 10 and 20 km, although many events are also observed at depths up to 40 km

and 33 km). These events have been removed from the analysis. Nonetheless, a sufficient number of samples was available to perform a reasonable statistical analysis (Fig. 4).

6.2 Source mechanism

Geometry of the source is fully described by the focal mechanism parameters strike, dip and rake. While strike and dip uniquely describe fault orientation, rake is used to further specify the rupture kinematic (normal, thrust, strike-slip or oblique). Such source parameters can be estimated directly by the analysis of fault-plane solutions from moment tensor inversion of earthquake recordings, or indirectly by the analysis of local and regional stress regimes and existing geological structures. We based our considerations on the geological and seismological literature available for the area (see Sect. 5).

The tectonic regime in the study region is mostly extensional, although a minor but not negligible transform component is also observed in many areas. Normal faulting style was modelled by imposing a standard (constant) dip angle of 60° and rake of 90°, adding where necessary a strike-slip component by allowing oblique strike on the fault plane. Since in most cases precise information on average slip direction was not available, either left lateral (−45°) and right-lateral (−135°) rake components were allowed with equal probability.

The overall strike distribution was calibrated by performing statistical analysis on the outcropping fault structures available from the database of Macgregor (2015). To do this, we split fault traces into segments of fixed length (1 km), in order to weight segments of different length proportionately, but also to avoid issues related to arbitrary segmentation of main faults. Segment statistics were then used to constrain average strike orientation in each zone (e.g. Fig. 5). In a few cases, bimodal (and even more complex) distributions were found, which are likely due to a mixed tectonic regime. In those cases where no sufficient data were available to constrain a predominant orientation, we based our judgement on available moment tensor solutions and tectonic regime descriptions from literature, or alternatively by using an isotropic (equal-probability) distribution.

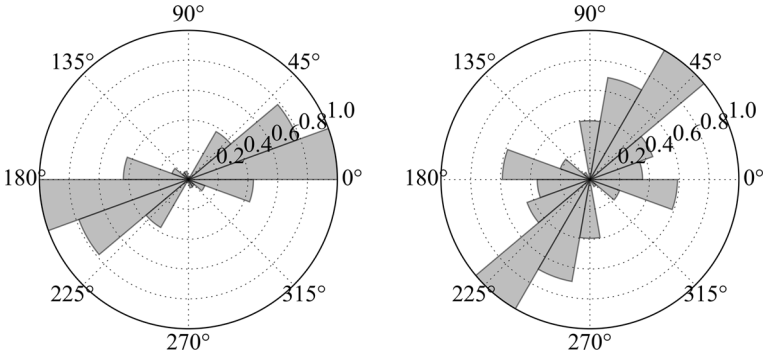

Fig. 5 Distribution of fault orientation (*strike*) for two example source zones (4, 7). Input information is from the fault database of Macgregor (2015)

6.3 Seismicity analysis

6.3.1 Completeness analysis

Earthquake catalogue completeness (Rydelek and Sacks 1989; Woessner and Wiemer 2005) is evaluated for different temporal periods and magnitude ranges by integration of two complementary procedures. First, results from the unsupervised Stepp (1971) algorithm are evaluated, using the implementation available within the GEM's Hazard Modeller Toolkit (HMTK) (Weatherill 2014a). This method, however, proved to be unstable, giving potentially erroneous results in the case of sparse and irregular data coverage, as it is unfortunately the case for Sub-Saharan Africa. As subsequent refinement, therefore, we have manually adjusted the retrieved completeness thresholds by evaluating the variability of occurrence rates over time (e.g. Fig. 6) and by investigating its impact on the magnitude frequency distribution (as discussed in the next section). Several iterations of progressive adjustment were required to converge to a stable and satisfactory result. In a first stage, a unique completeness was evaluated for the whole study area (e.g. Fig. 6). From that, results were subsequently refined for each source zone group to account for local specificities (e.g. due to non-uniform spatial distribution of seismicity), while keeping the total rate balance unmodified.

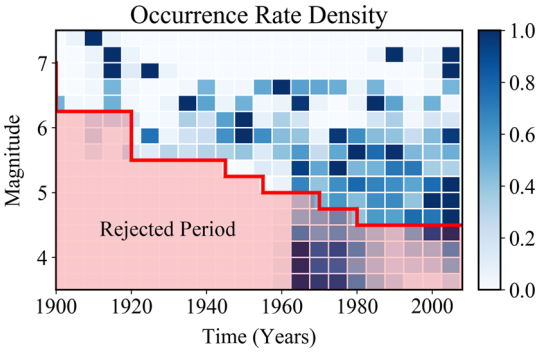

Fig. 6 Magnitude-time density plot of the SSA-GEM catalogue. Normalised rates are computed for fixed time windows of 5 years and for a 0.25 magnitude unit increment. Incomplete data periods (and other periods rejected from further interpretation) are marked with the *pink* shaded area

6.3.2 *Magnitude-frequency distribution*

Seismicity in each area source is assumed to follow a double truncated Gutenberg–Richter magnitude occurrence relation (or magnitude-frequency distribution, MFD). Lower truncation is arbitrarily assigned to M_W 4.5 (lowest magnitude threshold considered capable of generating damage) for all zones. Upper truncation is defined as the magnitude of the largest earthquake assumed possible (or, rather, plausible) for an area. A different maximum magnitude (M_{MAX}) estimate is derived independently for each source group as the largest observed event plus an arbitrary—although quite conservative—increment of 0.5 magnitude units.

Gutenberg–Richter *b*-values have been calibrated for the whole catalogue and independently for each source group. Conversely, occurrence rates (*a*-values) have been calculated separately for each source zone by imposing the previously calibrated *b*-values (Table 4). This strategy was necessary given the limited amount of data available for the study area, and particularly for those zones of quite limited extension.

In addition to using standard and well-established approaches (e.g. Weichert's maximum likelihood method; Weichert 1980), we tested and compared results from an alternative strategy we developed based on direct inversion of incremental (non-cumulative)

Table 4 Calibrated seismicity parameters for each source zone, divided by tectonic group

Group	Source	*a*-value	*b*-value	M-max
1	2	4.83	1.02	7.2
	3	5.38		
2	1	4.48	0.95	7.5
	4	4.18		
	22	3.70		
3	7	4.00	1.02	6.9
	7.1	4.23		
	14	4.34		
	20	3.31		
4	5	4.22	1.02	7.9
	6	4.89		
	8	4.84		
	9	4.93		
	18	4.40		
5	10	3.90	0.99	6.9
	10.1	3.92		
	11	3.51		
	11.1	3.93		
	12	4.05		
	12.1	4.13		
	13	4.08		
	13.1	3.99		
6	15	5.31	1.16	7.4
	16	5.45		
	17	4.77		

Sources marked with 0.1 represent overlapping layers within a background zone

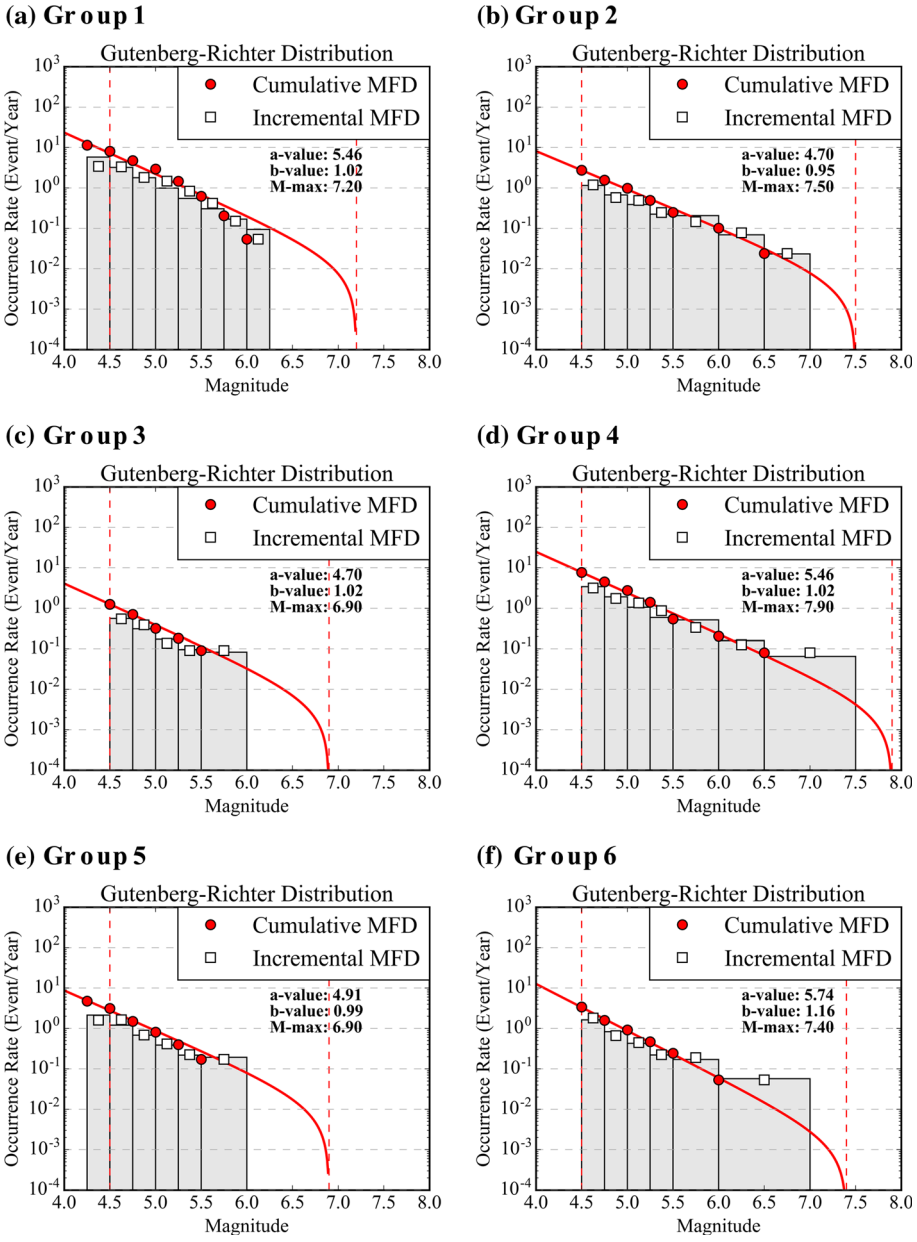

Fig. 7 Gutenberg–Richter magnitude occurrence relations of each tectonic group computed from the declustered SSA-GEM catalogue. *White squares* and *red dots* are respectively the observed incremental and cumulative occurrence rates, while the *grey* histogram and the *red line* represent the incremental and cumulative rates from the inverted Gutenberg–Richter relation. It must be noted that the width of non-cumulative magnitude bins is not uniform, as this is not a requirement of the fitting method

earthquake occurrences using a nonlinear least-square approach. Seismicity parameters (*a*- and *b*-values) are obtained by minimizing the residuals between observed rates in discrete magnitude bins and a theoretical non-cumulative MFD model (e.g. Fig. 7). Such strategy is advantageous in that target observations are independent and the results are therefore not affected by discontinuous earthquake records, as for the case of uncertain completeness of reported large magnitudes. Moreover, a variety of a priori constraints (e.g. fixed *b*-value or maximum magnitude) can easily be included in the analysis.

6.3.3 Earthquake rate balancing

In order to avoid duplicate counts of events on overlapping zones (e.g. 12 and 12.1), an appropriate redistribution of seismic rates is necessary. Background events have to be removed from the rates computed for the topmost overlapping layer, so that joint calculation of the occurrence rates for the two zones will keep the total balance unmodified. In order to do so, the unit-area background rate is obtained by counting the occurrences in the background region not falling also into the overlapping layer. This can be done by simple subtraction of the total events observed in the two zones. The background rate is then removed from the occurrence of the overlapping zone after rescaling by local area extension. For simplicity, we limited this procedure to just one single overlapping zone, but such a strategy can nonetheless be extended to the use of several layers, each delimited by contouring the average density level of events over the area. This last approach would be an intermediate approach between standard distributed and gridded seismicity models, where the occurrence rates for a unit area could vary over the zone, while keeping the total rate balance unmodified.

7 Logic tree implementation

While the aleatory (or random) component of the model uncertainty is generally taken into account through the hazard integral, the epistemic component, which is related to the available level of knowledge and/or the adopted initial assumptions and simplifications, can be quantified by using a logic-tree strategy. In a logic-tree approach, different interpretations of the model components are considered concurrently. Statistical analysis is performed a posteriori on the weighted outcome of each model realisation (or logic-tree branch). *OpenQuake*-engine allows the use of separate branching levels, each of those representing a separate contribution to uncertainty. A multi-level strategy ensures the full exploration of the model variability by computation of all possible permutations of those model parameters affected by epistemic uncertainty. We applied this strategy to account for the difference between existing ground motion prediction models and for the variability of source parameters not directly constrained by available data.

7.1 Ground motion prediction equations

The optimum strategy for the selection of the most representative Ground Motion Prediction Equations (GMPE) is the direct comparison of empirical ground motion estimates with observed earthquake recordings in a sufficiently representative range of magnitudes and distances. The GEM Ground Motion Toolkit (GMTK) offers a set of simple functionalities to pursue this goal (Weatherill 2014b). Unfortunately, Sub-Saharan Africa is affected by a severe lack of data availability. The use of *AfricaArray* networks did not contribute significantly, as no large magnitude events were recorded and the lack of recordings in the near

to intermediate distance range (<50 km). For these reasons, we had to rely for GMPE selection on a simpler—but less accurate—selection criteria, based on direct evaluation and comparison of GMPE features, such as the tectonic setting, the type and quality of data used for calibration, and the suitability of the functional form (Cotton et al. 2006).

In a first round, sixteen GMPEs were selected as possible candidates from a worldwide database, covering four different tectonic contexts: active shallow crust (ASC), stable continental crust (SCC), cratons (CRT) and volcanic areas (VLC). However, ground motion prediction equations from CRT and VLC settings were excluded, because of the questionable applicability to the investigated area and the lack of available data to perform ad-hoc ground-motion analysis. This last issue is particularly critical in case of volcano-related seismicity, which is nonetheless a possibly significant contribution to seismic hazard at specific sites. Once more data is made available, it is advisable that this component will be progressively integrated into the model.

In a second attempt, GMPEs for ASC and SCC were assigned to different source groups. While we used ASC GMPEs for areas involving plate boundary segmentation, SCC GMPEs were used to model ground motion in all intra-plate areas. The rationale behind this choice is the evolution of the African rifting. Given the relatively young age of the process, it might be expected that extra-rift regions are less exposed to asthenospheric upwelling, and therefore able to preserve a mechanical behaviour and a seismicity footprint typical of stable continental areas. However, after some sensitivity test calculation, we found that using a sharp separation between regions of different tectonic setting led to unjustifiably large differences in the computed ground motion across certain zone boundaries. In order to minimize such effects, while retaining the assumption of diversity in crustal attenuation and stress-drop, we proceeded with an alternative approach.

The current logic-tree model was restricted to the use of four GMPEs, respectively two for active shallow crust (Chiou and Youngs 2014; Akkar et al. 2014) and two for stable continental conditions (Atkinson and Boore 2006; Pezeshk et al. 2011). We then assigned all of the selected GMPEs to each source zone, but allowed the corresponding logic-tree weight to vary in agreement with the likelihood for each specific tectonic type. Assignment of weights was agreed on the basis of the direct judgement of local seismotectonic conditions by a pool of experts from the region. The full list of weights is summarised in Table 5. Zones sharing the same weighting scheme have then been clustered into four main groups (named A to D) to reduce the total number of end-branches into the logic tree implementation. In Fig. 8 a comparison of the response spectra from the selected GMPE is presented for a range of magnitude and distance values.

Table 5 Weighting scheme used for the GMPE logic tree

Group ID	Source ID	CY	AK	AB	PZ
A	1, 2, 3, 4, 17	0.5	0.5	0	0
B	5, 6, 8, 9, 1, 8, 22	0.375	0.375	0.125	0.125
C	15	0.25	0.25	0.25	0.25
D	7, 10, 11, 12, 13, 14, 16, 20	0.125	0.125	0.375	0.375

Source zones sharing the same weights are grouped into four main categories (A–D). Four attenuation models were applied (*CY* Chiou and Youngs 2014; *AK* Akkar et al. 2014; *AB* Atkinson and Boore 2006; *PZ* Pezeshk et al. 2011)

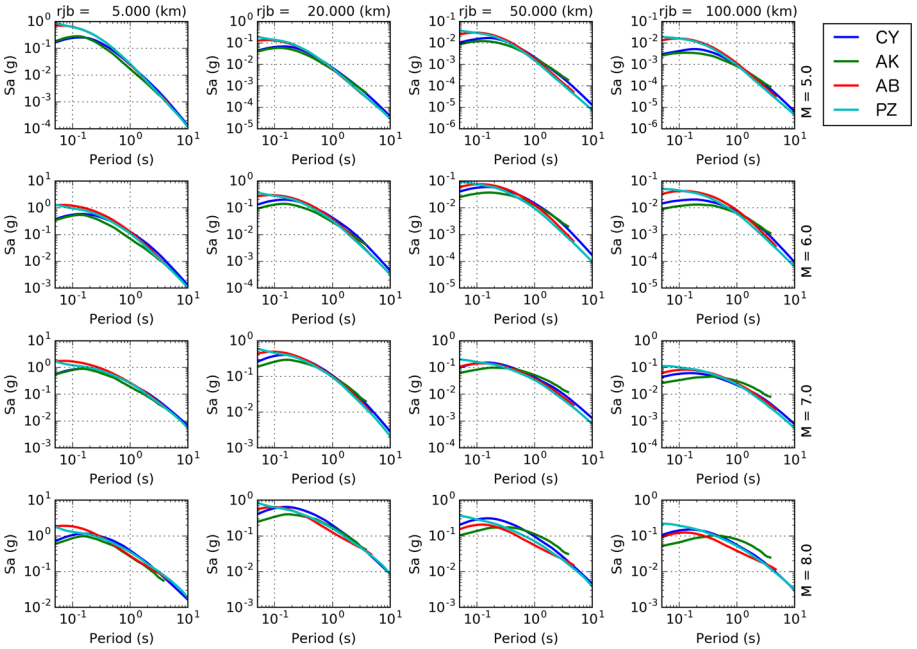

Fig. 8 Comparison between response spectra predicted by the four selected GMPEs as a function of M_W magnitude (*rows*, M_W 5–M_W 8) and Joyner–Boore distance (*columns*, 5–100 km). Attenuation models are abbreviated as in Table 5

7.2 Source model uncertainty

Given the explorative nature and the initial goals of the present study, the source model logic tree has currently a single master branch that includes the area source zonation previously described. Using a single zonation model has a clear impact on the epistemic variability of the hazard results. We envisage the integration of alternative area source interpretations as a possible extension of this study, as the result of the contribution of a wider community of African scientists.

On top of that, additional branching levels have been implemented to describe the epistemic variability of the assumed maximum magnitude of each zone (e.g. Fig. 9). Given the poor constraints available for its definition, maximum magnitude is assumed to have a relative possible error of ± 0.2, assigned empirically with a certain level of conservatism. The higher weight (0.5) is assigned to the original unmodified magnitude estimate, while edge values (± 0.2) have a lower probability of 0.25 each. We presently did not account for uncertainty on occurrence rates and b-values, although we acknowledge this is a necessary subsequent improvement of the model, which would eventually impact the epistemic variability of the results.

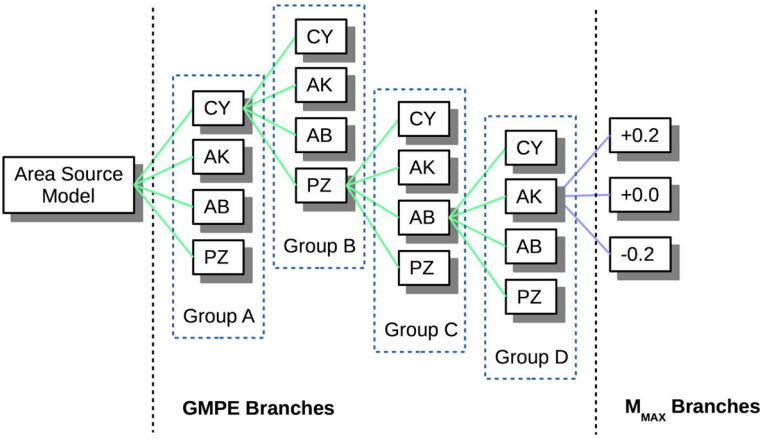

Fig. 9 Schematic representation of branch permutation for the current logic-tree implementation. Four independent branching levels are first used to characterise the four main tectonic groups (A–B–C–D) for the area. For each group, different weighting is then assigned to the selected GMPEs (see Table 5). An additional branching level is finally implemented to explore the variability of source parameters within each group. Given the explorative nature of the study, we presently only consider the uncertainty on maximum magnitude (M_{max})

8 PSHA results

8.1 *OpenQuake* settings

Hazard computations have been performed using the *OpenQuake*-engine (Version 2.0) through the available calculator for distributed seismicity (see OpenQuake Reference Manual for details on available calculators). The investigation area consists of a mesh of 79,109 sites spaced at approximately 10 km. Such area includes all earthquake source zones described in Sect. 3, plus a buffer region of not less than 100 km. For each site of the mesh, free rock conditions are assumed, with a fixed 30-metre averaged shear-wave velocity (Vs_{30}) reference of 600 m/s (corresponding to stiff-soil transition in Eurocode8 [CEN 2004] and NEHRP [BSSC 2003] classification). We choose this rock condition because we believe it is more representative of a realistic outcropping rock (which should include a certain degree of fracturing and weathering) than the more commonly used hard rock assumption with a Vs_{30} equal to (or higher than) 800 m/s. The choice of the reference condition is nonetheless quite arbitrary, and adjustments can still be applied subsequently to conform to a different reference.

Target ground motion intensity for calculation is 5% damped response spectral acceleration (in g), estimated for probabilities of exceedance (PoE) of 10 and 2% within an investigation time of 50 years. This corresponds respectively to return periods of about 475 and 2475 years. Due to the substantial lack of historical records for proper calibration of the large magnitude rates, we avoid using longer return periods.

According to the possibilities of the selected GMPEs, spectral acceleration has been computed at PGA and for the response spectral periods of 0.05 s, 0.1 s, 0.2 s, 0.5 s, 1 s and 2 s. Ground motion distribution has been conservatively truncated at $\pm 3\sigma$. Output of the calculation are mean and quantile (0.15, 0.5 and 0.85) hazard curves at each site, together

with Uniform Hazard Spectra (UHS) and hazard maps, which are described in the next sections.

8.2 Calculation outputs

Hazard calculations have been performed for each site of the investigation grid. For the sake of conciseness, however, in the following we illustrate hazard results for four selected African capitals, which are considered to be significant for risk analysis:

- Addis Ababa (Ethiopia);
- Kampala (Uganda);
- Nairobi (Kenya);
- Bujumbura (Burundi).

8.2.1 Earthquake hazard curves

Hazard curves are calculated for fixed acceleration values between 0.005 g and 2.13 g for each prescribed spectral period (including PGA). Acceleration corresponding to the target probability of exceedance(s) is subsequently extracted from the curves by linear interpolation. The mean hazard curves for different spectral periods at the four example locations are presented in Fig. 10. The unusual behaviour of the hazard curves in Kampala at long periods should be noted; this is likely due to concurrence of GMPEs for shallow crust and stable continental conditions, which affect the various probabilities differently.

8.2.2 Earthquake hazard maps

A series of hazard maps have been produced for different spectral periods and PoEs. In the following we will focus on discussing the results for a 10% PoE in 50 years (Fig. 11), as the associated mean return period is commonly used to characterise the seismic behaviour of non-critical facilities.

Largest spectral accelerations are found for periods of 0.1 and 0.2 s along the Western Branch of the EARS (0.51 g), particularly for source zones 6 (Lakes Albert to Kivu) and 8 (Lake Tanganyika). Moderate accelerations (less than 0.35 g) are expected in the Afar region (zone 1) in northern Ethiopia. Southern Ethiopia (zone 4) presents levels (0.24 g at 0.2 s) that are comparable to western EARS (zone 15) and the side seismic belts of Zambia (zone 12). Remaining portions of the rift are affected by an overall lower hazard, with accelerations generally lower than 0.2 g.

8.2.3 Uniform hazard spectra

Uniform Hazard Spectra (UHS) are computed by collecting ground motion for a given probability of exceedance over a spectrum of different response periods. This representation is useful to highlight those periods where larger spectral acceleration is expected. It is however important to stress that UHS cannot be directly used to model local scenarios (e.g. for the selection of a reference earthquake), as the different spectral ordinates might be (and likely are) linked to different controlling events (e.g. Reiter 1990). For that purpose, a disaggregation procedure is best suited.

In Fig. 12 mean and quantile UHS are shown for the four selected African capitals (10% PoE in 50 years). It is evident that periods between 0.1 and 0.2 s make a considerable

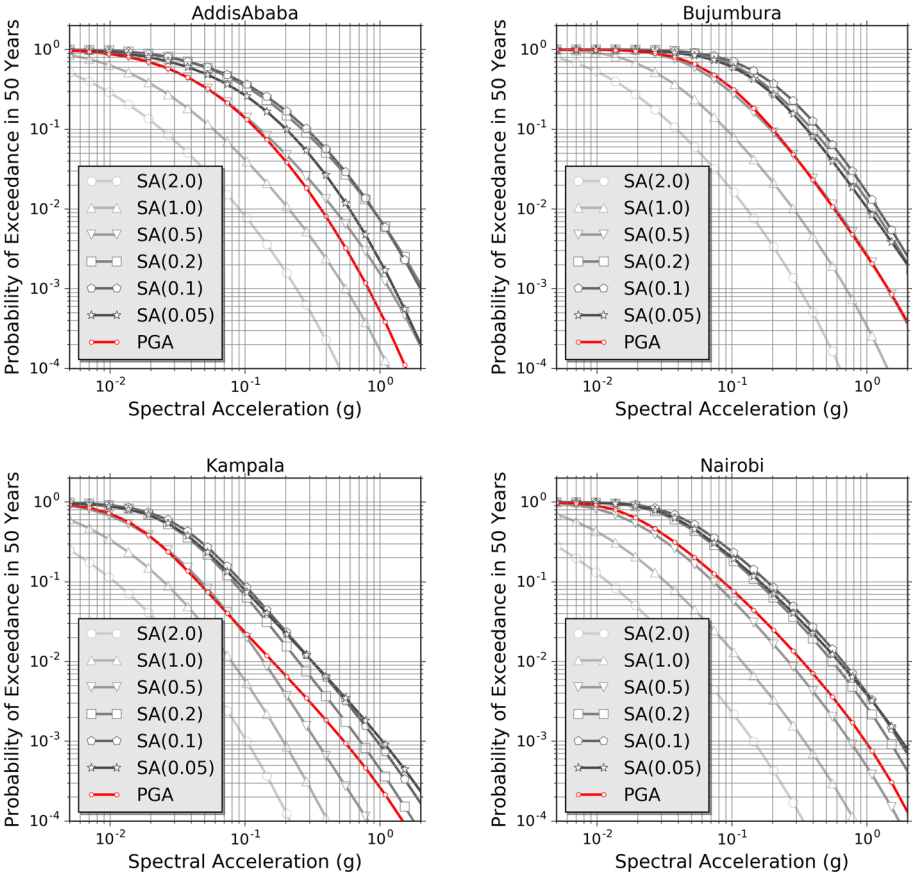

Fig. 10 Mean hazard curves computed for a range of spectral periods, including PGA (in *red*), at four example African cities

contribution to the hazard, as the largest ground accelerations are to be expected in this range. Among possible explanations, this phenomenon may be related to the residual contribution in the ground motion model of seismic site-effects (e.g. high-frequency resonance) not adequately accounted for in the GMPE site term, particularly when a single soil-class predictor—such as the Vs_{30}—is used (e.g. Poggi et al. 2017). The affected period range is, however, significant from an engineering perspective, as it matches the resonance response of typical buildings in urban environments.

9 Discussion and conclusions

The SSA PSHA model is generally consistent with the previous regional model from the GSHAP project (Midzi et al. 1999), however with some noticeable differences. Starting from north, the largest PGA (10% PoE in 50 years) of the SSA model is observed in Djibouti (0.22 g) and at the border with Somalia. The value nearly matches the GSHAP prediction for the same area. Different values are, however, obtained in northern Ethiopia

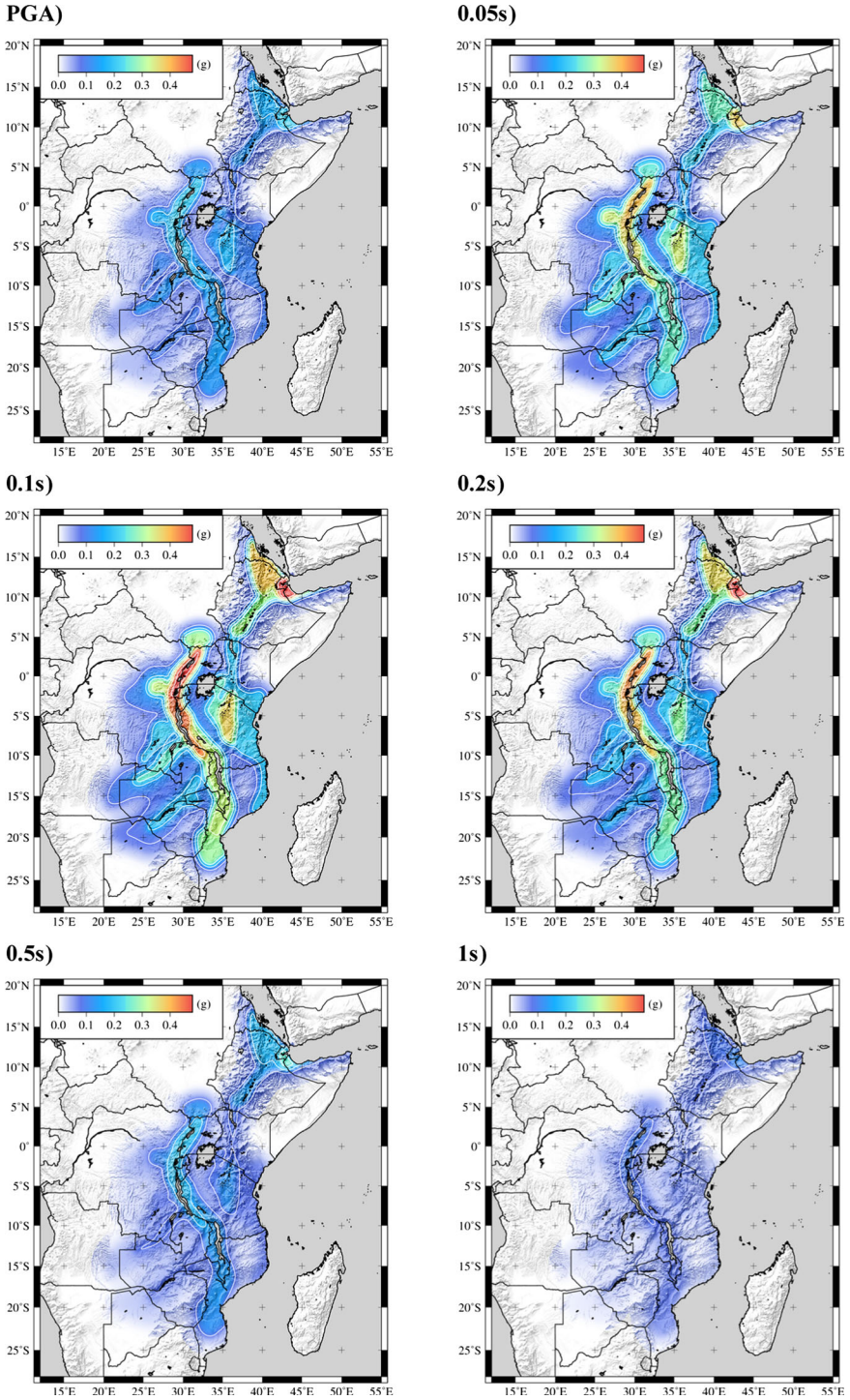

Fig. 11 Map of spectral acceleration (g) for 10% probability of exceedance in 50 years

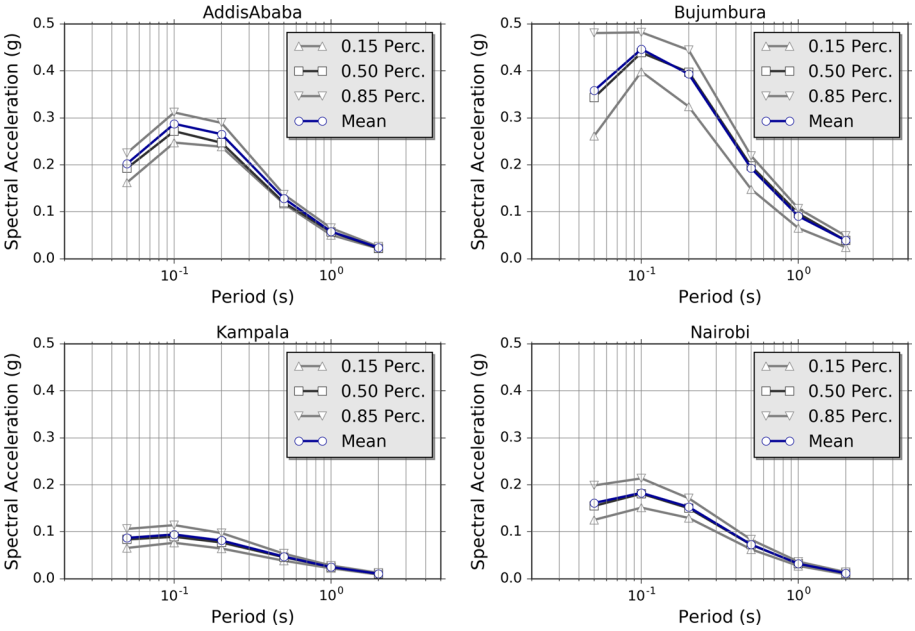

Fig. 12 Mean and quantile Uniform Hazard Spectra (UHS) computed at the four selected African capitals for 10% probability of exceedance in 50 years (475 year return period). It is worth noting how the mean and the 0.5 percentile curves are generally in good agreement and overlapping, with the only noticeable exception of Addis Ababa in the 0.1–0.2 s spectral period range

and the Afar region, where the current model predicts a somewhat lower acceleration (0.16 g) than GSHAP (around 0.2 g). This is likely due to the different approach used to represent multiple area sources at the Afar triple junction.

Moving southward, the maximum acceleration in the Ethiopian plateau shows similar values (0.13 g) for the two models. Following the western branch of the EARS, the biggest difference is found in the south Sudan cluster (Juba region), where a difference in acceleration of about 0.08 g is observed. This is again likely due to the different modelling strategy of the area sources. GSHAP does not define an *ad-hoc* source zone to describe the cluster, therefore transferring the moderate seismicity of the lakes region also to the north. A similar situation is found towards the south, where the SSA model predicts a slightly lower acceleration for the Lake Tanganyika (0.2 g) if compared to the region of the northern lakes (Kivu, Edward and Albert). Conversely, the southern tail of the western branch (e.g. in Malawi) shows a considerably higher acceleration (0.15 g) than GSHAP (0.08 g), which we could explain in term of the expanded catalogue and different calibration of seismicity parameters.

Again, the eastern branch of the EARS has similar maximum accelerations to the GSHAP model in northern Tanzania, but some differences are observed in the intra-plate background seismicity of the Victoria micro-plate and southern Kenya. A feature of GSHAP that does not appear in the SSA model is a seismic belt in southern Zimbabwe. No evidence of seismicity is observable from the SSA-GEM catalogue for this feature, although a system of faults is documented in the literature.

The major issue affecting the SSA model is the shortage of strong-motion recordings within a sufficient distance to be used for selection and validation of existing ground

motion prediction models. In this study, a choice of suitable GMPEs have been based on the crustal structure of the EARS, relying on a set of assumptions from seismotectonic considerations that still need full validation. Future installation of new strong-motion stations at potentially hazardous sites and the strengthening of existing seismic networks will be an essential advancement to verify the applicability of existing ground motion prediction models and to promote the development of new locally-calibrated ones. Moreover, the availability of strong-motion recordings will support site-specific hazard studies, which require empirical data for the calibration and verification of numerical seismic-response models. Note, however, that calculation of site-specific hazard is impractical for such a large area. For city scenarios, however, the use of site-specific information from local investigations and microzonation studies is highly advisable. This is a possible second-phase extension of this study.

By analysing the completeness periods of the SSA-GEM catalogue, it is also evident that additional information is required to fill significant gaps in the past earthquake record. This issue is particularly evident for the large-magnitude events, whose occurrence rate estimates could be improved by new historical and macroseismic studies, as well as by progressive integration of paleoseismic and geodetic information, which are nowadays of very limited availability. To compensate for this lack of information, GEM is presently evaluating the potentialities of a strain rate model recently developed by Stamps et al. (2015). We plan to use the inferred geodetic strain rates to derive estimates of total scalar moment release, subsequently needed to constrain earthquake recurrence relationships for both area (as distributed seismicity) and fault source models. The rates obtained indirectly from strain rates and more classically derived from the available seismic catalogues will be compared and combined into a unique mixed earthquake recurrence model, subsequently used as the base for seismic hazard calculations.

Improvements are also possible in the design of the logic tree structure. Up to now, the only considered epistemic variability of the source model is about the uncertainty of M_{MAX}, while neglecting any possible error on *b*-value and occurrence rate estimates. This was mostly done to reduce the complexity of the logic-tree structure—by limiting the total number of parameter permutations—but it might have the drawback to underestimate the true hazard in some regions. For future developments it is therefore advisable to perform a round of sensitivity tests to explore the impact of such epistemic variability on the results, as well as the integration of alternative source zonation models, to account for the subjective choice of regional discretization.

Finally, it is important to highlight that, although the presented model have been calibrated on the most recent information available for Sub-Saharan Africa and using state of the art tools for seismic hazard analysis, our interpretations should not be regarded as a final product, but should rather be regarded as a starting point for the development of continuously-updated and dynamically-improved snapshot of the current seismic hazard knowledge for the region. To make this process feasible, however, it is essential to ensure that all the model-related information (e.g. source models, SSA-catalogue, documentation) is open and publicly available to the community. GEM will support this policy by hosting model files into the GEM world database of open models.

One additional mention should be made of the 3 April 2017 earthquake in central Botswana (MW 6.5). Investigation is ongoing into the characteristics of seismogenic source of the earthquake, appearing to be somewhat deeper than typical for events in this region. The felt intensity data, however, suggest a slow rate of attenuation but a level of ground shaking that conforms neither to that of active nor stable ground motion models. This, perhaps coincidentally, aligns with the rationale adopted in the current ground motion

logic tree in which GMPEs from older stable continental regions are combined with those from active regions. Occurring after the completion of this model, and with its location beyond the limits of the target region considered here, this event highlights the persistent low-level threat that earthquakes can pose to society even in regions of low seismicity.

Acknowledgements This study is made possible by the generous support of the American people through the United States Agency for International Development (USAID). The contents are the responsibility of GEM and do not necessarily reflect the views of USAID or the United States Government. *AfricaArray* projects that have provided seismicity information used for this study have been supported by the U.S. National Science Foundation. We would like to thank Dr. Duncan Macgregor for having provided the African fault database. A special thanks goes also to Dr. Dario Slejko and the anonymous reviewer for their appreciation for our work and their insightful suggestions.

References

Adams A, Nyblade A, Weeraratne D (2012) Upper mantle shear wave velocity structure beneath the East African Plateau: evidence for a deep, plateau-wide low velocity anomaly. Geophys J Int 189:123–142

Akkar S, Sandikkaya MA, Bommer JJ (2014) Empirical ground-motion models for point- and extended-source crustal earthquake scenarios in Europe and the Middle East. Bull Earthq Eng 12:359–387

Ambraseys NN (1991a) The Rukwa earthquake of 13 Dec. 1910 in E. Africa. Terra Nova 3:203–208

Ambraseys NN (1991b) Earthquake hazard in the Kenya Rift: the Subukia earthquake 1928. Geophys J Int 105:253–269

Ambraseys NN, Adams RD (1991) Reappraisal of major African earthquakes, south of 20°N, 1900–1930. Nat Hazards 4:389–419

Atkinson G, Boore D (2006) Earthquake ground-motion prediction equations for eastern North America. Bull Seismol Soc Am 96:2181–2205

Ayele A, Nyblade AA, Langston CA, Cara M, Leveque J (2006) New evidence for Afro-Arabian plate separation in southern Afar. In: Yirgu G, Ebinger CJ, Maguire PKH (eds) The Afar volcanic province within the East African Rift System. Geol. Soc. Lond. Spec. Publ. 259:254–263

Barth A, Wenzel F, Giardini D (2007) Frequency sensitive moment tensor inversion for light to moderate magnitude earthquakes in eastern Africa. Geophys Res Lett 34:L15302

Brazier RA, Nyblade AA, Florentin J (2005) Focal mechanisms and the stress regime in NE and SW Tanzania. Geophys Res Lett 32:L14315. doi:10.1029/2005GL023156

Brazier R, Miao Q, Nyblade A, Ayele A, Langston C (2008) Local magnitude scale for the Ethiopian Plateau. Bull Seismol Soc Am 98:2341–2348. doi:10.1785/0120070266

Brzev S, Scawthorn C, Charleson AW, Allen L, Greene M, Jaiswal K, Silva V (2013) GEM building taxonomy version 2.0. GEM Technical Report 2013-02 V1.0.0, p 188, GEM Foundation, Pavia, Italy. doi:10.13117/GEM.EXP-MOD.TR2013.02

BSSC (2003) The 2003 NEHRP Recommended provisions for new buildings and other structures. Part 1: provisions (FEMA 450), Building Seismic Safety Council. www.bssconline.org

Casey M, Ebinger C, Keir D, Gloagen R, Mohamed R (2006) Strain accommodation in transitional rifts: extension by magma intrusion and faulting in the Ethiopian rift magmatic segment. In: Yirgu G, Ebinger CJ, Maguire PKH (eds) The Afar volcanic province within the East African Rift System. Geol. Soc. Lond. Spec. Publ. 259: 143–163

CEN (2004) Eurocode 8: design of structures for earthquake resistance—part 1: general rules, seismic actions and rules for buildings. European Committee for Standardization, British Standard BS EN 1998-1:2004: E, 219

Chesley JT, Rudnick RL, Lee CT (1999) Re-Os systematics of mantle xenoliths from the East African Rift: age, structure, and history of the Tanzanian craton. Geochim Cosmochim Acta 63:1203–1227

Chiou BS-J, Youngs RR (2014) Update of the chiou and youngs NGA model for the average horizontal component of peak ground motion and response spectra. Earthq Sp 30:1117–1153

Chorowicz J (2005) The East African rift system. J Afr Earth Sci 43:379–410

Cotton F, Scherbaum F, Bommer JJ, Bungum H (2006) Criteria for selecting and adjusting ground motion models for specific target regions: application to central Europe and rock sites. J Seismol 10:137–156

Craig TJ, Jackson JA, Priestley K, McKenzie D (2011) Earthquake distribution patterns in Africa: their relationship to variations in lithospheric and geological structure, and their rheological implications. Geophys J Int 185:403–434

Dawson JB (1992) Neogene tectonics and volcanicity in the North Tanzania sector of the Gregory Rift Valley: contrasts with the Kenya sector. Tectonophysics 204:81–92
Delvaux D, Barth A (2010) African stress pattern from formal inversion of focal mechanism data. Tectonophysics 482:105–128
Delvaux D, Kervyn F, Macheyeki AS, Temu EB (2012) Geodynamic significance of TRM segment in East African Rift (W-Tanzania): active tectonics and paleostress in the Ufipa plateau and Rukwa basin. J Struct Geol 37:161–180
Delvaux D, Mulumba J-L, Fiama Bondo S, Kervyn F, Havenith H-B (2016) Seismic hazard assessment of the Kivu rift segment based on a new seismotectonic zonation model (Western Branch, East African Rift system). J Afr Earth Sci AVCoR. doi:10.1016/j.jafrearsci.2016.10.004
d'Oreye N, Fernandez J, Gonzalez P, Kervyn F, Wauthier C, Frischknecht C, Calais E, Heleno S, Cayol V, Oyen A, Marinkovic P (2008) Systematic InSAR monitoring of African active volcanic zones: what we have learned in three years, or an harvest beyond our expectations. In: Second workshop on use of remote sensing techniques for monitoring volcanoes and seismogenic areas, USEReST 2008, 57–62
Durrheim RJ (2016) African earthquakes. In: Mulugeta G, Simelane T (eds) Natural and human-induced hazards and disasters in Africa. Africa Institute of South Africa, Pretoria, pp 16–42
Edwards B, Allmann B, Fäh D, Clinton J (2010) Automatic computation of moment magnitudes for small earthquakes and the scaling of local to moment magnitude. Geophys J Int 183:407–420
Ekström G, Nettles M, Dziewonski AM (2012) The global CMT project 2004–2010: centroid-moment tensors for 13,017 earthquakes. Phys Earth Planet Inter 200–201:1–9
Engdahl ER, Villaseñor A (2002) Global Seismicity: 1900-1999. In: Lee WHK, Kanamori H, Jennings PC, Kisslinger C (eds) International Handbook of Earthquake and Engineering Seismology, Part A, Chapter 41. Academic Press, New York, pp 665–690
Fenton CH, Bommer JJ (2006) The M_W 7.0 Machaze Mozambique earthquake of 23 February 2006. Seismol Res Lett 77:425–439
Field EH, Jordan TH, Cornell CA (2003) OpenSHA—a developing community-modeling environment for seismic hazard analysis. Seismol Res Lett 74:406–419
Franke D, Jokat W, Ladage S, Stollhofen H, Klimke J, Lutz R, Mahanhane ES, Ehrhardt A, Schreckenberger B (2015) The offshore East African Rift System: structural framework at the toe of a juvenile rift. Tectonics 34:2086–2104
Furman TK, Kaleta J, Bryce J, Hanan B (2006) Tertiary mafic lava of Turkana, Kenya: constraints on EAST African plume structure and the occurrence of high μ volcanism in Africa. J Petrol 47:1221–1244
Gardner JK, Knopoff L (1974) Is the sequence of earthquakes in Southern California, with aftershocks removed, Poissonian? Bull Seismol Soc Am 64:1363–1367
Grimison NL, Chen WP (1988) Earthquakes in Davie Ridge-Madagascar region and the southern Nubian-Somalian plate boundary. J Geophys Res 93:10439–10450
Gurnis M, Mittovica J, Ritsema J, Van Hest HJ (2000) Constraining mantle density structure using geological evidence of surface uplift rates: the case of African super-plume. Geochem Geophys Geosyst 1:10220
Hansen S, Nyblade AA, Benoit M (2012) Mantle structure beneath Africa and Arabia from adaptively parameterized P-wave tomography: implications for the origin of Cenozoic Afro-Arabian tectonism. Earth Planet Sci Lett 319–320:23–34
Hartnady CJH (1990) Seismicity and plate boundary evolution in Southeastern Africa. S Afr J Sci 93:473–484
Hartnady CJH (2002) Earthquake hazard in Africa: perspectives on the Nubia-Somalia boundary. S Afr J Sci 98:425–428
Hartnady CJH, Ben-Avrahan HZ, Rogers J (1992) Deep-ocean basin basins and submarine rises of the continental margin of south-eastern Africa: new geological research. S Afr J Sci 88:534–539
ISC (2013) International Seismological Centre, On-line Bulletin. http://www.isc.ac.uk. Int Seismol Cent, Thatcham, United Kingdom
Kebede F, Kulhanek O (1991) Recent seismicity of the East African rift system and its implications. Phys Earth Planet Inter 68:259–273
Keir D, Hamling J, Ayele A, Calais E, Wright T (2009) Evidence for focused magmatic accretion at segment centers from lateral dike injection captured beneath the Red Sea Rift in Afar. Geology 37:59–62
Kipata ML, Delvaux D, Sebagenzi MN, Cailteux J-J, Sintubin M (2013) Brittle tectonic and stress field evolution in the Pan-African Lufilian arc and its foreland (Katanga, DRC): from orogenic compression to extensional collapse, transpressional inversion and transition to rifting. Geol Belg 16:1–17
Langston CA, Brazier RA, Nyblade AA, Owens TJ (1998) Local magnitude scale and seismicity rate for Tanzania, East Africa. Bull Seismol Soc Am 88:712–721

Lithgow-Berteloni C, Silver PG (1998) Dynamic topography, plate driving forces and the African superswell. Nature 395:269–272
Lubkowski Z, Villani M, Coates K, Jirouskova N, Willis M (2014) Seismic design considerations for East Africa. In: Second European conference on earthquake engineering and seismology, 25–29 August 2014, p 14
Macgregor D (2015) History of the development of the East African Rift System: a series of interpreted maps through time. J Afr Earth Sci 101:232–252
Macheyeki AS, Delvaux D, De Batist M, Mruma A (2008) Fault kinematics and tectonic stress in the seismically active Manyara-Dodoma Rift segment in Central Tanzania—implications for the East African Rift. J Afr Earth Sci 51:163–188
Mavonga T (2007) Some characteristics of aftershock sequences of major earthquakes from 1994 to 2002 in the Kivu Province, Western Rift Valley of Africa. Tectonophysics 439:1–12
Mavonga T, Durrheim RJ (2009) Probabilistic seismic hazard assessment for the Democratic Republic of Congo and surrounding areas. S Afr J Geol 112:329–342
McConnell RB (1980) A resurgent taphrogenic lineament of Precambrian origin in eastern Africa. J Geol Soc Lond 137:483–489
McDougall I, Brown FH (2009) Timing of volcanism and evolution of northern Kenya Rift. Geol Mag 146:34–47
McGuire RK (2004) Seismic hazard and risk analysis. Earthqu Eng Res Inst, Oakland
Midzi V, Manzunzu B (2014) Large recorded earthquakes in sub-Saharan Africa. In: Ismail-Zadeh A, Urrutia-Fucagauchi J, Kijko A, Zaliapin I (eds) Extreme natural hazards, disaster risks and societal implications. Cambridge University Press, Cambridge
Midzi V, Hlatywayo DJ, Chapola LS, Kebede F, Atakan K, Lombe DK, Turyomurugyendo G, Tugume FA (1999) Seismic hazard assessment in eastern and Southern Africa. Ann Geophys 42:1067–1083
Mulibo GD, Nyblade AA (2013) Mantle transition zone thinning beneath eastern Africa: evidence for a whole-mantle superplume structure. Geophys Res Lett 40:3562–3566
Mulibo GD, Nyblade AA (2016) The seismotectonics of southeastern Tanzania: implications for the propagation of the Eastern Branch of the East African Rift. Tectonophysics 974:20–30
Mulwa JK, Kimata F, Suzuki S, Kuria ZN (2014) The seismicity in Kenya (East Africa) for the period 1906–2010: a review. J Afr Earth Sci 89:72–78
Nyblade AA, Langston CA (1995) East African earthquakes below 20 km depth and their implications for crustal structure. Geophys J Int 121:49–62
Nyblade AA, Robinson SW (1994) The African superswell. Geophys Res Lett 21:765–768
Pagani M, Monelli D, Weatherill G, Danciu L, Crowley H, Silva V, Henshaw P, Butler L, Nastasi M, Panzeri L, Simionato M, Viganò D (2014) OpenQuake-engine: an open hazard (and risk) software for the global earthquake model. Seismol Res Lett 85:692–702
Petit C, Ebinger C (2000) Flexure and mechanical behaviour of cratonic lithosphere: gravity models of the East African and Baikal rifts. J Geophys Res 105:19151–19162
Pezeshk S, Zandieh A, Tavakoli B (2011) Hybrid empirical ground-motion prediction equations for eastern North America using NGA models and updated seismological parameters. Bull Seismol Soc Am 101:1859–1870
Pik R, Marty B, Carignan J, Lave J (2003) Stability of the upper Nile drainage network (Ethiopia) deduced from (U–Th)/He thermochronometry: implication for uplift and erosion of the Afar plume dome. Earth Planet Sci Lett 215:73–88
Poggi V, Edwards B, Fäh D (2017) A comparative analysis of site-specific response spectral amplification models. Phys Chem Earth 98:16–26 (**Special issue**)
Reiter L (1990) Earthquake hazard analysis. Columbia University Press, New York, p 254
Ritsema JH, Van Hest HJ, Woodhouse JH (1998) Complex shear wave velocity structure imaged beneath Africa and Iceland. Science 286:1925–1928
Roberts EM, Stevens NJ, O'Connor PM, Dirks PHGM, Gottfried MD, Clyde WC, Armstrong RA, Kemp AIS, Hemming S (2012) Initiation of the Western Branch of the East African Rift, coeval with the eastern Branch. Nat Geosci 5:289–294
Rydelek PA, Sacks JS (1989) Testing the completeness of earthquake catalogues and the hypothesis of self-similarity. Nature 337:249–251
Saria E, Calais E, Stamps DS, Delvaux D, Hartnady CJH (2014) Present-day kinematics of the East African Rift. J Geophys Res 119:3584–3600. doi:10.1002/2013JB010901
Shudofsky GN (1985) Source mechanisms and focal depths of East African earthquakes using the Rayleigh-wave inversion and body-wave modelling. Geophys J R Astron Soc 83:563–634
Simmons NA, Forte AM, Grand SP (2007) Thermochemical structure and dynamics of the African superplume. Geophys Res Lett 34(L02301):2006G. doi:10.1029/L028009

Stamps DS, Saria E, Kreemer C (2015) Sub-Saharan Africa geodetic strain rate model 1.0. GEM Technical report

Stepp JC (1971) An investigation of earthquake risk in the Puget Sound area by use of the type I distribution of largest extremes. Ph.D. thesis, Pennsylvania State University

Storchak DA, Di Giacomo D, Bondár I, Engdahl ER, Harris J, Lee WHK, Villaseñor A, Bormann P (2013) Public Release of the ISC-GEM Global Instrumental Earthquake Catalogue (1900-2009). Seismol Res Lett 84:810–815

Storchak DA, Di Giacomo D, Engdahl ER, Harris J, Bondár I, Lee WHK, Bormann P, Villaseñor A (2015) The ISC-GEM global instrumental earthquake catalogue (1900–2009). Introd Phys Earth Planet Int 239:48–63

Studt FE, Cornet J, Buttgenbach H (1908) Carte geologique du Katanga et notes descriptive. Am Musee Congo, Ser. 2, 1

Tanaka K, Horiuchi S, Sato T, Zana N (1980) The earthquake generating stresses in the Western Rift Valley of Africa. J Phys Earth 28:45–57

Uhrhammer R (1986) Characteristics of Northern and Central California seismicity. Earthq Notes 57:21

USGS (2016) M5.9–22 km NE of Nsunga, Tanzania. U.S. Geological Survey—earthquake hazards Program. http://earthquake.usgs.gov/earthquakes/eventpage/us10006nkx#executive. Accessed 12 Sept 2016

USNRC (2012) Practical implementation guidelines for SSHAC Level 3 and 4 hazard studies. Technical report, p 235. US Nuclear Regulatory Commission

Van Stiphout T, Zhuang J, Marsan D (2012) Theme V—models and techniques for analysing seismicity. Technical report. Community online resource for statistical seismicity analysis. doi:10.5078/corssa-52382934

Vilanova SP, Nemser ES, Besana-Ostman GM, Bezzeghoud M, Borges JF, Da Silveira AB, Cabral J, Carvalho J, Cunha PP, Dias RP, Madeira J, Lopes FC, Oliveira CS, Perea H, García-Mayordomo J, Wong I, Arvidsson R, Fonseca JFBD (2014) Incorporating descriptive metadata into seismic source zone models for seismic-hazard assessment: a case study of the Azores-West Iberian region. Bull Seismol Soc Am 104:1212–1229

Vittori E, Delvaux D, Kervyn F (1997) Kanda fault: a major seismogenic element west of the Rukwa Rift (East Africa: Tanzania). J Geophys 24:139–153

Weatherill GA (2014a) OpenQuake hazard modeller's toolkit—user guide. Glob Earthq Model (GEM). Technical Report. doi:10.13117/GEM.OPENQUAKE.MAN.HMTK.01

Weatherill GA (2014b) OpenQuake ground motion toolkit—user guide. Glob Earthq Model (GEM). Technical Report. doi:10.13117/GEM.OPENQUAKE.MAN.GMTK.01

Weatherill GA, Pagani M, Garcia J (2016) Exploring earthquake databases for the creation of magnitude-homogeneous catalogues: tools for application on a regional and global scale. Geophys J Int 206:1652–1676

Weichert DH (1980) Estimation of the earthquake recurrence parameters for unequal observation periods for different magnitudes. Bull Seismol Soc Am 70:1337–1346

Woessner J, Wiemer S (2005) Assessing the quality of earthquake catalogues: estimating the magnitude of completeness and its uncertainty. Bull Seismol Soc Am 95:684–698

Wolfenden E, Ebinger C, Yiirgu G, Deino A, Ayalew D (2004) Evolution of the northern Main Ethiopian Rift: birth of a triple junction. Earth Planet Sci Lett 224:213–228

Worku A (2014) The status of basic design ground motion provisions in seismic design codes of Sub-Saharan African countries. J S Afr Inst Civ Eng 56:40–53

Yang Z, Chen WP (2010) Earthquakes along the East African Rift System: a multiscale, system-wide perspective. J Geophys Res 115:B12309

Zana N, Wafula M, Lukaya N, Batabolo M (2004) The Kabalo earthquake in DR Congo on September 11, 1992: field observations and damages. Quelques résultats de Recherches en Géophysique. Centre de Recherches et Pédagogie appliqués (C. R. P. A), I.P.N, Kinshasa, 77–89